Eur. J. Mineral., 34, 365–374, 2022
https://doi.org/10.5194/ejm-34-365-2022

European Journal of Mineralogy
Open Access

Graulichite-(La), $LaFe^{3+}_3(AsO_4)_2(OH)_6$, a new addition to the alunite supergroup from the Patte d'Oie mine, Bou Skour mining district, Morocco

Cristian Biagioni[1], Marco E. Ciriotti[2,3], Georges Favreau[4], Daniela Mauro[5], and Federica Zaccarini[6]

[1]Dipartimento di Scienze della Terra, Università di Pisa, Via Santa Maria 53, 56126 Pisa, Italy
[2]Dipartimento di Scienze della Terra, Università degli Studi di Torino, Via Valperga Caluso 35, 10125 Turin, Italy
[3]Associazione Micro-mineralogica Italiana, Via San Pietro 55, 10073 Devesi-Ciriè, Italy
[4]Association Française de Microminéralogie, Avenue Jean Monnet, 13090 Aix-en-Provence, France
[5]Museo di Storia Naturale, Università di Pisa, Via Roma 79, 56011 Calci, Italy
[6]Faculty of Science, Physical and Geological Sciences, Universiti Brunei Darussalam, Jalan Tungku Link, BE1410 Gadong, Brunei

Correspondence: Cristian Biagioni (cristian.biagioni@unipi.it)

Received: 22 March 2022 – Accepted: 4 June 2022 – Published: 27 June 2022

Abstract. The new mineral species graulichite-(La), ideally $LaFe^{3+}_3(AsO_4)_2(OH)_6$, has been discovered in the Patte d'Oie mine, Bou Skour mining district, Morocco. It occurs as yellow rhombohedral crystals, up to 0.1 mm in size, with a resinous luster, associated with malachite, agardite-(La), conichalcite, and a still undetermined REE carbonate. Crystals are chemically zoned and two homogeneous domains were identified, corresponding to the empirical chemical formulae (calculated on the basis of 6 cations per formula unit, assuming the occurrence of 14 O atoms) $(La_{0.34}Ce_{0.20}Ca_{0.11}Sr_{0.07}Pb_{0.05}K_{0.04})_{\Sigma 0.81}(Fe^{3+}_{2.16}Al_{0.84}Cu_{0.20})_{\Sigma 3.20}(As_{1.23}P_{0.39}S_{0.37})_{\Sigma 1.99}O_{14}H_{6.13}$ (domain #1) and $(La_{0.38}Ce_{0.22}Sr_{0.10}Ca_{0.09}Pb_{0.05}K_{0.06})_{\Sigma 0.90}(Fe^{3+}_{2.60}Al_{0.49}Cu_{0.20})_{\Sigma 3.29}(As_{0.91}P_{0.50}S_{0.40})_{\Sigma 1.81}O_{14}H_{6.53}$ (domain #2). Single-crystal unit-cell parameters are $a = 7.252(13)$, $c = 16.77(3)$ Å, $V = 764(3)$ Å^3, space group $R\text{-}3m$. The eight strongest reflections in the observed X-ray powder diffraction pattern are (d in Å, visually estimated intensity): 5.86, medium; 3.045, strong; 2.511, medium-weak; 2.239, medium; 1.960, medium-weak; 1.813, medium-weak; 1.689, medium-weak; 1.478, medium. Graulichite-(La) belongs to the dussertite group within the alunite supergroup. It is the La analogue of graulichite-(Ce) and the Fe^{3+} analogue of arsenoflorencite-(La).

1 Introduction

The alunite supergroup is currently formed by more than 50 different mineral species, characterized by the general chemical formula $DG_3(TX_4)_2X'_6$, where D can be represented by monovalent, divalent, trivalent, and tetravalent cations, as well as vacancy; G is usually a trivalent cation and less frequently a divalent one; T is a hexavalent or pentavalent cation, and rarely Si^{4+}; and X and X′ are O^{2-}, $(OH)^-$, (H_2O), or F^-. Species characterized by $T = S^{6+}$ or As^{5+} are typically formed during the weathering of sulfide deposits (e.g., Dutrizac and Jambor, 2000) and may play a relevant environmental role in controlling the fate of potentially toxic elements (PTE), including As. This element typically occurs in minerals belonging to the dussertite and beudantite groups within the alunite supergroup (Bayliss et al., 2010). Arsenic can also partially replace S in jarosite in acid mine drainage systems, with important implications on the As mobility (e.g., Gieré et al., 2003; Martín Romero et al., 2010; Burton et al., 2021). Moreover, the identification of

alunite supergroup minerals may explain other geogenic PTE anomalies in some localities (e.g., Mauro et al., 2021).

In the framework of an ongoing study of the mineralogy of the Bou Skour mining district, Morocco, carried out by the Association Française de Microminéralogie, small yellow rhombohedral crystals were observed on a centimeter-sized specimen of malachite grown on iron oxides and associated with an agardite-like mineral. Preliminary chemical and micro-Raman data showed that these crystals could correspond to the La analogue of graulichite-(Ce). Further studies confirmed the preliminary results, and the mineral and its name were approved by the Commission on New Minerals, Nomenclature and Classification of the International Mineralogical Association (CNMNC-IMA) under voting number 2020-093. The name highlights its relations with graulichite-(Ce) (Hatert et al., 2003), in accord with the nomenclature of REE-bearing minerals (Levinson, 1966; Bayliss and Levinson, 1988). Holotype material is deposited in the mineralogical collection of the Museo di Storia Naturale, University of Pisa, Via Roma 79, Calci (Pisa), under catalogue number 19924.

This paper describes the new mineral species graulichite-(La), briefly discussing its relations with other alunite supergroup minerals.

2 Occurrence and physical properties

Graulichite-(La) was found in the Patte d'Oie mine, Bou Skour mining district, in the Djebel Saghro mountain range, about 50 km southeast of Ouarzazate, Morocco. This mining district belongs to the Cu hydrothermal ore deposits located in the Anti-Atlas domain. In the Patte d'Oie mine, ore body is mainly formed by chalcopyrite with abundant bornite, chalcocite, galena, and tetrahedrite-group minerals, in quartz veins. This locality is well-known for its supergene minerals, e.g., agardite-(Y), first found at this locality in 1964 (Dietrich et al., 1969), azurite, cuprite, and wulfenite, the latter in bluish crystals (Dietrich, 1972; Dietrich and Favreau, 2005). A description of the mineralogy of this locality was given by Dietrich (1970).

A geological background can be found in Maacha et al. (2011) and El Azmi et al. (2014). The studied material was originally collected by Jacques Émile Dietrich in the active underground workings of the Patte d'Oie mine in the late 1960s, when he was a geologist in Morocco; the sample was then given to one of the authors (Georges Favreau) and kept as a part of his systematic collection.

Graulichite-(La) occurs as rhombohedral crystals, up to 0.1 mm in size, yellow in color (Fig. 1), with a light-yellow streak. Luster is resinous and fluorescence was not observed. It is brittle, with an irregular fracture. No cleavage or parting was observed. Hardness and density were not measured, owing to the small size of available crystals. Mohs hardness was estimated to be ~ 3.5, in agreement with other alunite supergroup minerals (e.g., Mills et al., 2010). As will be discussed below, crystals of graulichite-(La) are chemically inhomogeneous and the calculated density for the two observed homogeneous domains are 3.907 and 3.962 g cm^{-3} for domain #1 and #2, respectively. Notwithstanding its euhedral morphology, crystals are internally porous, as confirmed by polished sections showing only very thin laminae determining the external morphology (Fig. 2). This feature greatly complicated the full crystal-chemical investigation of this material, resulting in a low quality of collected data.

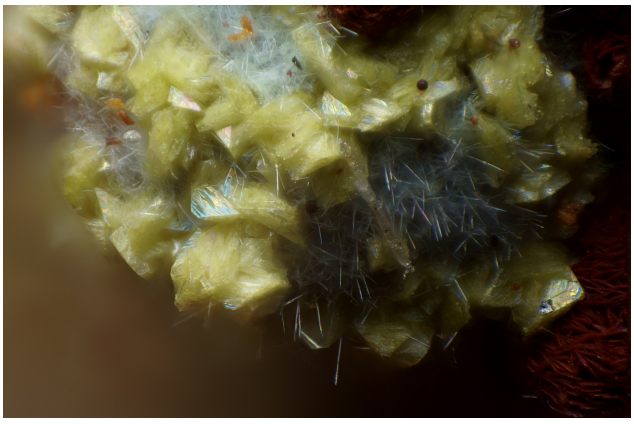

Figure 1. Graulichite-(La), as yellow rhombohedral crystals with thin needles of agardite-(La). Field of view: 0.5 mm. Collection Georges Favreau, photo Pierre Clolus.

Owing to the small amount of available material and its nature, only very basic optical observations were performed. Graulichite-(La) is transparent, with a very weak pleochroism from light yellow to yellow. As in graulichite-(Ce) (Hatert et al., 2003), birefringence was difficult to observe because interference colors are masked by the yellow color of the mineral. Mean refractive index, calculated according to the Gladstone–Dale relationship (Mandarino, 1979, 1981), is 1.889 and 1.928 for domains #1 and #2, respectively.

Graulichite-(La) is associated with malachite, agardite-(La), conichalcite, and a still undetermined synchysite-like REE carbonate. Its origin is related to the oxidation of primary ores exploited at the Patte d'Oie mine; the presence of REE in this secondary assemblage could be related to the interaction between acidic solutions formed during sulfide oxidation and minerals of the host rocks (andesite, granite).

3 Raman spectroscopy

Micro-Raman spectra of graulichite-(La) were collected in nearly back-scattered geometry with a Horiba Jobin-Yvon XploRA Plus apparatus, equipped with a motorized x–y stage and an Olympus BX41 microscope with a 50× objective. The 532 nm line of a solid-state laser was used. The minimum lateral and depth resolution was set to a few micrometers. The system was calibrated using the 520.6 cm^{-1} Ra-

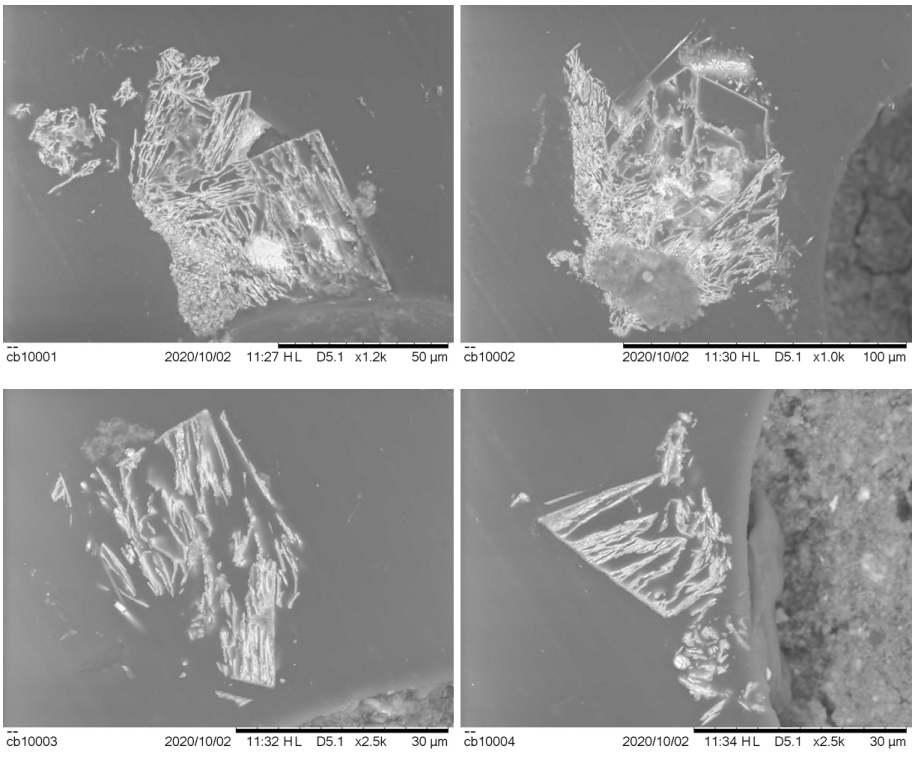

Figure 2. Backscattered electron images of polished crystals of graulichite-(La) embedded in epoxy, showing their porous nature.

man band of silicon before each experimental session. Spectra were collected through multiple acquisitions (3) with single counting times of 30 s, with the laser power filtered at 25 % (6.25 mW). Backscattered radiation was analyzed with a 1200 g mm^{-1} grating monochromator.

The Raman spectrum of graulichite-(La) and the band positions are shown in Fig. 3. The region between 100 and 1200 cm^{-1} can be divided into three regions. Between 700 and 1200 cm^{-1}, vibrational modes related to the occurrence of (AsO_4) and minor (PO_4) and (SO_4) groups can be observed. The strongest band at 846 cm^{-1} is related to the ν_1 mode of the (AsO_4) groups. Bands at 995 and 1092 cm^{-1} (the latter being broad) are likely due to the ν_1 and ν_3 modes of (SO_4) groups, as well as to the occurrence of (PO_4) groups. For instance, Frost et al. (2011) assigned bands between 996 and 1000 cm^{-1} observed in beudantite to the ν_1 mode of (SO_4) groups, and a series of bands between 1061 and 1155 cm^{-1} as due to the ν_3 modes of (SO_4) groups. In florencite-(La), Frost et al. (2013) proposed to identify a band at 987 cm^{-1} as due to (PO_4) symmetric stretching modes, whereas antisymmetric stretching modes were observed between 1064 and 1221 cm^{-1}. The band at 714 cm^{-1} in the Raman spectrum of graulichite-(La) may be interpreted as due to O–H deformation modes, in agreement with Frost et al. (2013), who reported a band at 716 cm^{-1} in florencite-(La). Between 350 and 700 cm^{-1}, the strongest band is at 466 cm^{-1}, attributed to the ν_4 mode of (AsO_4) groups; this band has a shoulder toward the lower wavenumbers, interpreted as due to the ν_2 mode of (SO_4) groups. The bands at 565 and 618 cm^{-1} may be interpreted as the ν_4 modes of (SO_4) groups, as well as the ν_2 modes of (PO_4) groups. The Raman bands below 350 cm^{-1} can be interpreted as M–O modes (e.g., the band at 330 cm^{-1} – Frost et al., 2013) and lattice vibrations.

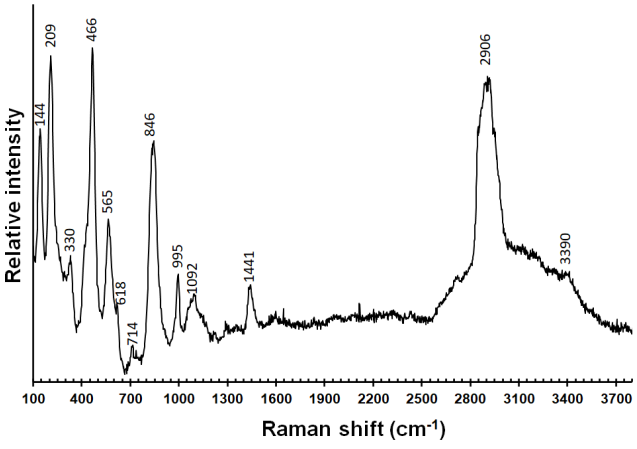

Figure 3. Raman spectrum of graulichite-(La). The position of observed bands is given (in cm^{-1}).

The O–H stretching region, between 2900 and 3800 cm^{-1}, is characterized by a broad and weak band, with a rela-

tively narrow spectral and very strong feature at 2906 cm^{-1}. Whereas the broad and weak band may be attributed to several kinds of O–H environments (it may be possible that both OH and H_2O occurs in the studied mineral, and that $(As,P)O_3(OH)$ groups may partially replace $(As,P)O_4$ groups), the band at 2906 cm^{-1} is not attributed. In addition, a band at 1441 cm^{-1} is observed. Similar features can be noted in the infrared spectrum of florencite-(La) reported by Frost et al. (2013) but not discussed. In addition, similar bands occur in the Raman spectrum of florencite-(La) reported by Repina et al. (2011). These authors interpreted the band at 2957 cm^{-1} as due to O–H stretching, whereas the bands in the region between 1400 and 1500 cm^{-1} are interpreted as due to the presence of CO_3 groups. Other possible interpretations of this band may be related to the possible occurrence of $(NH_4)^+$ groups or to the possibility of overtone bands. The former hypothesis is unlikely, because Raman spectroscopy is not very sensitive as regards the occurrence of N–H bending modes (e.g., Kampf et al., 2016; Biagioni et al., 2020) and the observed bands should indicate relatively high (NH_4) contents that should favor a significant expansion of the unit-cell volume with respect to graulichite-(Ce). Such an expansion was not observed. The possible interpretation of the band at 1441 cm^{-1} as due to overtones modes agrees with that given by Plášil et al. (2014), who interpreted a band at 1449 cm^{-1} as due to (SO_4) overtones.

4 Chemical data

Preliminary chemical analysis, performed using energy-dispersive spectrometry (EDS mode), revealed the occurrence of La, Ce, Ca, Sr, Fe, Al, Cu, As, P, and S as the elements with $Z > 8$ above the detection limit.

Quantitative chemical analyses were carried out using a Superprobe JEOL JXA 8200 electron microprobe (WDS mode, 20 kV, 10 nA, 1 µm beam diameter) at the Eugen F. Stumpfl laboratory (Leoben University, Austria). Standards (element, emission line) were as follows: anhydrite (S$K\alpha$), apatite (P$K\alpha$, Ca$K\alpha$), $PtAs_2$ (As$L\alpha$), corundum (Al$K\alpha$), hematite (Fe$K\alpha$), monazite (La$L\alpha$, Ce$L\alpha$), chalcopyrite (Cu$K\alpha$), strontianite (Sr$L\alpha$), galena (Pb$M\alpha$), and sanidine (K$K\alpha$). Counting times were 20 s for peaks and 10 s for left and right backgrounds, respectively. Every attempt to collect chemical data on the polished grains was unsuccessful, owing to the very small size of the lamellae embedded in epoxy (Fig. 2). Finally, chemical data were collected on the flat surface of an unpolished crystal of graulichite-(La). Low analytical total, after the addition of calculated H_2O, is probably due to the porous nature of the studied material and the poor quality of sample surface. Consequently, in addition to the measured values, chemical data normalized to sum = 100 wt % are given (Table 1).

Two chemically homogeneous domains (labeled #1 and #2) were identified. In agreement with Hatert et al. (2003), the chemical formulae of graulichite-(La) were calculated on the basis of 6 cations per formula unit, assuming the occurrence of 14 O atoms per formula unit (apfu); H content was estimated in order to achieve the electrostatic balance. Domain #1 corresponds to the chemical formula $(La_{0.34}Ce_{0.20}Ca_{0.11}Sr_{0.07}Pb_{0.05}K_{0.04})_{\Sigma 0.81}(Fe^{3+}_{2.16}Al_{0.84}Cu_{0.20})_{\Sigma 3.20}(As_{1.23}P_{0.39}S_{0.37})_{\Sigma 1.99}O_{14}H_{6.13}$, whereas domain #2 has the composition $(La_{0.38}Ce_{0.22}Sr_{0.10}Ca_{0.09}Pb_{0.05}K_{0.06})_{\Sigma 0.90}(Fe^{3+}_{2.60}Al_{0.49}Cu_{0.20})_{\Sigma 3.29}(As_{0.91}P_{0.50}S_{0.40})_{\Sigma 1.81}O_{14}H_{6.53}$. Both formulae led to the end-member composition $LaFe^{3+}_3(AsO_4)_2(OH)_6$. The ideal formula of graulichite-(La), $LaFe^{3+}_3(AsO_4)_2(OH)_6$, corresponds to (in wt %) As_2O_5 33.49, Fe_2O_3 34.90, La_2O_3 23.74, H_2O 7.88, total 100. Notwithstanding the low quality of chemical data, the mineral stoichiometry is consistent with the crystal chemistry of alunite-supergroup minerals.

5 X-ray crystallography

X-ray powder diffraction data were collected using a 114.6 mm Gandolfi camera and Ni-filtered Cu$K\alpha$ radiation. Table 2 gives the observed and the calculated X-ray powder diffraction patterns, compared with that of graulichite-(Ce) (Hatert et al., 2003). Unit-cell parameters, refined on the basis of 13 unequivocally indexed reflections using the software UnitCell (Holland and Redfern, 1997), are $a = 7.2469(9)$, $c = 16.767(2)$ Å, $V = 762.59(17)$ Å^3.

Several crystals of graulichite-(La) were tested, but they usually gave powder-like patterns, probably owing to the extreme fragility and porous nature of the available sample that formed a powdery material during the manipulation. Only one very thin lamina gave some spots suitable for single-crystal X-ray diffraction study. Similar difficulties were also encountered by Hatert et al. (2003) during their study of graulichite-(Ce). They described powder-like patterns, with diffuse streaks, owing to subparallel association of single individuals. Intensity data of graulichite-(La) were collected using a Bruker Apex II diffractometer equipped with a Photon II CCD area detector, and graphite-monochromatized Mo$K\alpha$ radiation (Dipartimento di Scienze della Terra, University of Pisa). The detector-to-crystal distance was 50 mm. A total of 336 frames was collected using ω scan modes, in 0.5° slices, with an exposure time of 120 s per frame. The data were corrected for Lorentz and polarization factors and absorption using the software package Apex3 (Bruker AXS Inc., 2016). Owing to the very small crystal size, only 118 reflections were measured up to $2\theta = 31.75°$, resulting in only 47 unique reflections. Unit-cell parameters are $a = 7.252(13)$, $c = 16.77(3)$ Å, $V = 764(3)$ Å^3. The $c : a$ ratio is 2.3125. These values can be compared with those reported by Hatert et al. (2003) for graulichite-(Ce), i.e., $a = 7.288(2)$, $c = 16.812(9)$ Å, $V = 773.3(6)$ Å^3. Systematic absences agree with the space group symmetry $R\bar{3}m$. The crystal structure of graulichite-(La) was refined using

Table 1. Chemical data (in wt %) for graulichite-(La).

	Domain #1 ($n = 4$)				Domain #2 ($n = 4$)			
Constituent	Mean	Range	e.s.d. (σ)	Norm. Data	Mean	Range	e.s.d. (σ)	Norm. Data
SO_3	3.90	3.69–4.05	0.16	4.98	4.40	3.90–5.18	0.56	5.26
P_2O_5	3.65	3.23–4.01	0.36	4.66	4.89	4.36–5.10	0.55	5.85
As_2O_5	18.55	18.18–18.84	0.28	23.68	14.48	13.86–15.40	0.73	17.31
Al_2O_3	5.63	5.54–5.79	0.11	7.19	3.41	2.91–3.70	0.36	4.08
Fe_2O_3	22.52	22.22–22.75	0.22	28.75	28.60	27.56–30.46	1.28	34.19
La_2O_3	7.16	6.90–7.30	0.18	9.14	8.59	8.26–8.96	0.35	10.27
Ce_2O_3	4.28	4.15–4.43	0.13	5.46	4.87	4.57–5.29	0.31	5.82
CaO	0.79	0.77–0.82	0.02	1.01	0.69	0.58–0.74	0.08	0.82
CuO	2.06	1.88–2.14	0.12	2.63	2.15	2.08–2.26	0.08	2.57
SrO	0.97	0.88–1.10	0.09	1.24	1.46	1.28–1.90	0.30	1.75
PbO	1.36	1.18–1.59	0.20	1.74	1.62	1.20–2.01	0.34	1.94
K_2O	0.25	0.23–0.26	0.02	0.32	0.40	0.35–0.52	0.08	0.48
H_2O_{calc}	7.22			9.22	8.10			9.68
Total	78.34			100.00	83.66			100.00

Note: n – number of spot analyses; e.s.d. – estimated standard deviation.

Table 2. X-ray powder diffraction data (d in Å) for graulichite-(La). Intensity and d_{hkl} were calculated using the software PowderCell 2.3 (Kraus and Nolze, 1996) on the basis of the structural model given in Table 4. Only the reflections with $I_{calc} > 5$ are given, if not observed. The eight strongest reflections are shown in bold. For the sake of comparison, the X-ray powder diffraction data of graulichite-(Ce) (Hatert et al., 2003) are reported.

d_{obs}	I_{obs}	d_{calc}	I_{calc}	$h\ k\ l$	Graulichite-(Ce)	
					d_{hkl}	I_{hkl}
5.86	**m**	5.88	60	1 0 1	5.906	25
3.611	w	3.626	37	1 1 0	3.636	40
–	–	3.086	14	0 2 1	3.088	10
3.045	**s**	3.042	100	1 1 3	3.052	100
2.953	w	2.941	17	2 0 2	–	–
2.791	w	2.795	17	0 0 6	2.792	30
2.511	**mw**	2.513	17	0 2 4	2.519	10
–	–	2.350	6	2 1 1	–	–
–	–	2.284	5	1 2 2	–	–
2.239	**m**	2.238	24	1 0 7	2.239	35
–	–	2.213	7	1 1 6	–	–
2.059	vw	2.066	2	2 1 4	–	–
1.960	**mw**	1.960	24	0 3 3	1.968	25
1.813	**mw**	1.813	23	2 2 0	1.817	35
1.689	**mw**	1.686	5	2 1 7	1.681	15
1.657	w	1.657	9	1 1 9	–	–
–	–	1.521	13	2 2 6	1.543	10
1.478	**m**	1.479	10	0 2 10	1.481	10

Note: observed intensities I_{obs} were visually estimated. s – strong; m – medium; mw – medium-weak; w – weak; vw – very weak.

Shelxl-2018 (Sheldrick, 2015) starting from the atomic coordinates of graulichite-(Ce) (Hatert et al., 2003). However, owing to the very low number of unique reflections, several constraints were imposed. Displacement parameters were refined isotropically, fixing their values to 0.030, 0.015, 0.020, and 0.025 Å^2, for the A, B, X, O(1), O(2), and OH sites, in agreement with values observed in graulichite-(Ce) (Hatert et al., 2003); site occupancy factors for the A, B, and X sites were refined using the following neutral scattering curves, taken from the International Tables for Crystallography (Wilson, 1992): La vs. □ at A, Fe vs. □ at B, and As vs. □ at X. In the final stages of the refinement, site occupancy factors were fixed, in order to reduce the number of refined parameters. Notwithstanding such an approach, the data / parameter ratio is poor, i.e., 6.71 (47 unique reflections and 7 refined parameters). After several cycles of isotropic refinement, the R_1 value converged to 0.0956 for 36 unique reflections with $F_o > 4\sigma(F_o)$. Details of data collection and refinement are given in Table 3. Atom coordinates and displacement parameters are reported in Table 4, whereas Table 5 reports selected bond distances.

6 Discussion

6.1 Crystal chemistry of graulichite-(La)

6.1.1 General features

As illustrated above, the crystal-chemical characterization of graulichite-(La) suffered because of the low quality of available material. Notwithstanding these shortcomings, all available data supported the proposed identification. The crystal structure of graulichite-(La) (Fig. 4) is isotypic with other

Table 3. Summary of parameters describing data collection and refinement for graulichite-(La).

Crystal data	
Crystal size (mm)	$0.040 \times 0.035 \times 0.030$
Cell setting, space group	Trigonal, $R\text{-}3m$
a (Å)	7.252(13)
c (Å)	16.77(3)
V (Å^3)	764(3)
Z	3
Data collection and refinement	
Radiation, wavelength (Å)	Mo $K\alpha$, $\lambda = 0.71073$
Temperature (K)	293(2)
$2\theta_{max}$ (°)	31.75
Measured reflections	118
Unique reflections	47
Reflections with $F_o > 4\sigma(F_o)$	36
R_{int}	0.0563
$R\sigma$	0.0726
Range of h, k, l	$-5 \le h \le 5$, $-4 \le k \le 4$, $-12 \le l \le 12$
R [$F_o > 4\sigma(F_o)$]	0.0956
R (all data)	0.1222
wR (on F_o^2)*	0.2162
Goof	1.237
Number of least-squares parameters	7
Maximum and minimum residual peak (e Å^{-3})	1.68 (at 0.68 Å from A) −1.50 (at 0.84 Å from A)

* $w = 1/[\sigma^2(F_o^2) + (0.0529P)^2 + 514.5002P]$.

Table 4. Sites, Wyckoff positions, site occupancy factors (s.o.f.), fractional atomic coordinates, and isotropic displacement parameters (in Å^2) for graulichite-(La).

Site	Wyckoff position	s.o.f.	x/a	y/b	z/c	U_{iso}
A	3a	$La_{0.95}$	0	0	0	0.030
B	9d	$Fe_{0.94}$	1/2	1/2	1/2	0.015
X	18f	$As_{0.70}$	0	0	0.3163(13)	0.020
O(1)	18f	$O_{1.00}$	0	0	0.415(5)	0.025
O(2)	18h	$O_{1.00}$	0.219(4)	−0.219(4)	−0.052(3)	0.025
OH	18h	$O_{1.00}$	0.120(5)	−0.120(5)	0.132(2)	0.025

alunite supergroup minerals, e.g., graulichite-(Ce) and other members of the dussertite group. It can be described as formed by layers of BO_6 octahedra, bonded through corner-sharing, giving rise to a planar network of triangular clusters delimiting hexagonal voids (such a network is described as hexagonal tungsten bronze, HTB – e.g., Grey et al., 2006). Such layers are decorated, on both sides, by XO_4 tetrahedra. The connection between successive layers, along c, is due to the 12-fold coordination A sites.

6.1.2 Cation sites

The A site shows an average bond distance of 2.78 Å, to be compared with 2.74 Å reported by Hatert et al. (2003) for graulichite-(Ce) and 2.682 Å observed by Mills et al. (2010) in arsenoflorencite-(La). Crystal structure refinement indicates a site scattering value corresponding to ∼ 54 electrons per formula unit (epfu). Chemical data show similar La / (La + Ce) atomic ratios in both the observed chemically homogeneous domains (i.e., ∼ 0.63), with the main difference being related to the amount of vacancy, i.e., 0.19 and 0.09 apfu. However, taking into account the low quality of chemical data, the occurrence of vacancy and its amount cannot be quantified confidently. If one assumes that no vacancy occurs, a hypothetical A site population could be $La_{0.43}Ce_{0.25}Ca_{0.11}Sr_{0.10}Pb_{0.06}K_{0.05}$, corresponding to 50.88 epfu, slightly less than the refined value. Assuming such a hypothetical site population and using the bond parameters of Gagné and Hawthorne (2015), the bond-valence

Table 5. Selected bond distances (in Å) for graulichite-(La).

A	−OH	2.67(5) × 6	*B*	−OH	1.958(19) × 4	*X*	−O(2)	1.56(5) × 3
	−O(2)	2.88(5) × 6		−O(2)	2.03(4) × 2		−O(1)	1.65(9)
	Mean	2.78		Mean	1.98		Mean	1.58

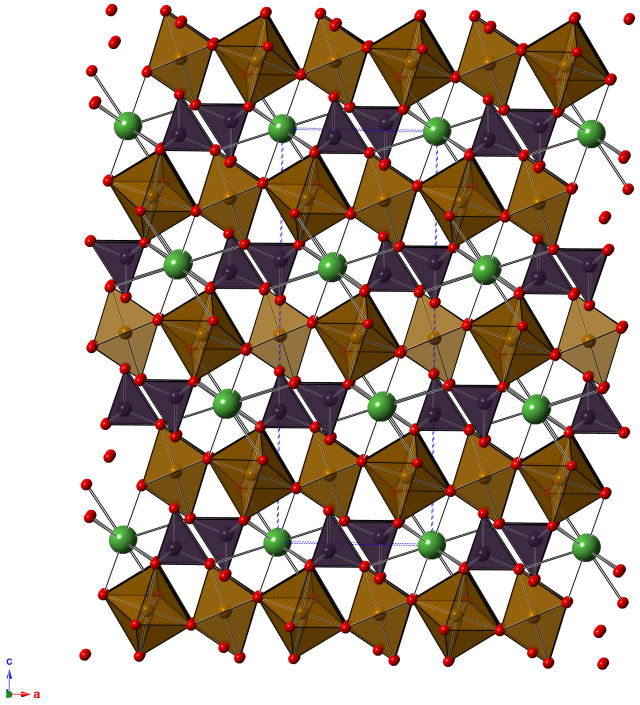

Figure 4. Crystal structure of graulichite-(La), as seen down *b*. Brown and violet polyhedra represent the *B*- and *X*-centered sites, whereas green and red circles are the *A* and O(1), O(2), and OH sites, respectively.

sum at the *A* site would be 2.22 valence unit (v.u.), to be compared with a theoretical value of 2.63 v.u. (Table 6).

The *B* site has an octahedral coordination, with four *B*–(OH) bonds (1.96 Å) and two slightly longer apical bonds with O(2) (2.03 Å). The average bond length, 1.98 Å, is similar to the ⟨*B*–O⟩ distance observed in graulichite-(Ce), 1.99 Å (Hatert et al., 2003). Using the ionic radii given by Shannon (1976) for $^{[VI]}Fe^{3+}$, $^{[VI]}Al^{3+}$, $^{[VI]}Cu^{2+}$, and $^{[III]}O^{2-}$ and normalizing the sum of Fe^{3+}, Al, and Cu^{2+} to 3 apfu, the calculated bond distances of 1.98 and 1.99 Å can be obtained for chemical domains #1 and #2, respectively. Refined site scattering (73.2 epfu) agrees with the chemical composition of domain #2; indeed, normalizing the content of Fe^{3+}, Al, and Cu^{2+} to 3 apfu, one obtains $(Fe_{2.38}Al_{0.45}Cu_{0.18})$, corresponding to a calculated site scattering of 73.0 epfu. Domain #1 has a calculated *B* site scattering of 68.4 epfu. Bond-valence sum at the *B* site is 3.20 v.u., larger than the theoretical value of 2.94 v.u.

The *X* site is a mixed (As, P, S) site. Its average ⟨*X*–O⟩ distance, 1.58 Å, is shorter than that observed in graulichite-(Ce) (1.68 Å) and agrees with the partial replacement of As^{5+} (⟨As–ϕ⟩ = 1.687 Å – Majzlan et al., 2014) with the smaller cations P^{5+} (⟨P–ϕ⟩ = 1.537 Å – Huminicki and Hawthorne, 2002) and S^{6+} (1.473 Å – Hawthorne et al., 2000). Coupling the information about ⟨*X*–O⟩ distance and refined site scattering (46.1 epfu), one can calculate the site population $(As_{0.86}P_{0.48}S_{0.66})_{\Sigma 2.00}$, which has more S than is suggested by the chemical data. Assuming this occupancy, bond valence at the *X* site is 5.49 v.u., to be compared with the theoretical value of 5.33 v.u. In alunite-structure type, the XO_4 tetrahedron shows a short *X*–O(1) bond and three longer *X*–O(2) bonds. For instance, in graulichite-(La), *X*–O(1) is 1.660(19) Å, whereas *X*–O(2) is longer, i.e., 1.690(12) Å (Hatert et al., 2003). In the studied sample, such a situation is apparently inverted, with *X*–O(1) longer than the three symmetry-related *X*–O(2) bonds, i.e., 1.65(9) vs. 1.56(5) Å, respectively. However, considering the large experimental uncertainty affecting the structural data of graulichite-(La), due to the low quality of the structure refinement, it is very probable that such an inversion in the bond length distribution is an artifact.

6.1.3 Anion sites

The three anion sites O(1), O(2), and OH have a bond-valence sum (BVS) of 1.14, 2.11, and 1.31 v.u. The O(1) site is an acceptor of H bonds from three symmetrically related OH, with O···O distance of 2.81 Å, corresponding to a bond strength, calculated according to Ferraris and Ivaldi (1988) of 0.18 v.u. Consequently, the corrected BVS for O(1) and OH, after considering the H bonds, are 1.68 and 1.13 v.u., agreeing with the occurrence of O^{2-} and $(OH)^{-}$ at these two sites. The underbonding at O(1) could be related to the possible occurrence of $(OH)^{-}$ at this position, as observed in other alunite supergroup minerals (e.g., Cooper and Hawthorne, 2012). In graulichite-(La), several substitutions occur with respect to the end-member formula $LaFe_3^{3+}(AsO_4)_2(OH)_6$. At the *A* site, trivalent REE are replaced by divalent (Ca, Sr, and Pb) and monovalent cations, whereas at the *B* site, $(Fe,Al)^{3+}$ is replaced by minor Cu^{2+}; finally, at the *X* site, As^{5+} and P^{5+} can be partially substituted by S^{6+}. Consequently, several heterovalent substitution mechanisms can be hypothesized. Indeed, one could suggest mechanisms involving only cations, e.g., $^{A,B}M^{3+} + {}^{X}M^{5+} = {}^{A,B}M^{2+} + {}^{X}M^{6+}$, or both cations and anions, e.g., $^{A,B}M^{3+} + {}^{O(1)}O^{2-} = {}^{A,B}M^{2+} + {}^{O(1)}(OH)^{-}$.

Table 6. Weighted bond valences (in valence units) in graulichite-(La).

Site	A	B	X	Σ_{anions}	Σ'_{anions}
O(1)			1.14	1.14	1.68
O(2)	$0.14^{\downarrow\times6}$	$0.52^{\downarrow\times2}$	$1.45^{\downarrow\times3}$	2.11	1.99
OH	$0.23^{\downarrow\times6}$	$^{2\times\rightarrow}0.54^{\downarrow\times4}$		1.31	1.13
$\Sigma_{cations}$	2.22	3.20	5.49		
Expected	2.69	2.94	5.33		

Note: left and right superscripts indicate the number of equivalent bonds involving anions and cations, respectively. Σ' is corrected for H bonds.

Table 7. Comparison between graulichite-(La) and other REE-bearing dussertite group minerals.

	Arsenoflorencite-(Ce)	Arsenoflorencite-(La)	Graulichite-(Ce)	Graulichite-(La)
Chemical formula	$CeAl_3(AsO_4)_2(OH)_6$	$LaAl_3(AsO_4)_2(OH)_6$	$CeFe^{3+}_3(AsO_4)_2(OH)_6$	$LaFe^{3+}_3(AsO_4)_2(OH)_6$
a (Å)	7.029	7.032	7.288	7.252
c (Å)	16.517	16.515	16.812	16.77
V (Å^3)	706.8	707.2	773.3	764
$\langle A–\varphi\rangle$ (Å)	No data available	2.682	2.744	2.78
Ce / (La + Ce)	0.60	0.24	0.87	0.37*
$\langle B–\varphi\rangle$ (Å)	No data available	1.894	1.989	1.98
Al / (Al + Fe)	1.00	0.98	0.14	0.15*
$\langle X–\varphi\rangle$ (Å)	No data available	1.668	1.682	1.58
As / (As + P + S)	0.74	0.90	0.94	0.43*
Ref.	Nickel and Temperly (1987)	Mills et al. (2010)	Hatert et al. (2003)	This work

* Using proposed site populations.

6.2 Relations with other species

Graulichite-(La) belongs to the dussertite group, a group of arsenate minerals within the alunite supergroup (Bayliss et al., 2010). This new mineral is the fourth REE-bearing member of this series, along with arsenoflorencite-(Ce), arsenoflorencite-(La), and graulichite-(Ce). Table 7 compares these phases. In addition, "arsenoflorencite-(Nd)" was described by Scharm et al. (1991) but never officially approved by the CNMNC-IMA. Among studied REE-bearing arsenates belonging to the dussertite group, graulichite-(La) has one of the lowest As / (As + P + S) atomic ratios. As discussed above some discrepancies between chemical and structural data occur; As is replaced by P and S, with the sum of As and P being larger than the S content, and As being the dominant cation of the dominant valence at the X site. Probably, the replacement of As by smaller P^{5+} and S^{6+} favors the contraction of unit-cell volume, $\Delta V = -1.20$ % with respect to graulichite-(Ce). Moreover, the occurrence of P^{5+} suggests the possibility that Fe^{3+} analogues of florencite-(Ce) and florencite-(La), both belonging to the plumbogummite group, may occur in nature.

Data availability. The Crystallographic Information File data of graulichite-(La) are available in the Supplement.

Supplement. The supplement related to this article is available online at: https://doi.org/10.5194/ejm-34-365-2022-supplement.

Author contributions. MEC and GF collected preliminary data. CB and DM carried out single-crystal X-ray diffraction and micro-Raman spectroscopy. FZ collected electron microprobe data. CB and DM wrote the paper, with input from MEC, GF, and FZ.

Competing interests. At least one of the (co-)authors is a member of the editorial board of *European Journal of Mineralogy*. The peer-review process was guided by an independent editor, and the authors also have no other competing interests to declare.

Disclaimer. Publisher's note: Copernicus Publications remains neutral with regard to jurisdictional claims in published maps and institutional affiliations.

Acknowledgements. Pierre Clolus is acknowledged for the photo of graulichite-(La). The University Centrum for Applied Geosciences (UCAG) is thanked for the access to the E. F. Stumpfl electron microprobe laboratory. The comments of Associate Editor Edward Grew and the reviewers Juraj Majzlan and Frédéric Hatert helped us in improving the paper.

Financial support. This research received support from the Ministero dell'Istruzione, dell'Università e della Ricerca through the project PRIN 2017 "TEOREM – deciphering geological processes using Terrestrial and Extraterrestrial ORE Minerals" (project no. 2017AK8C32).

Review statement. This paper was edited by Edward Grew and reviewed by Frédéric Hatert and Juraj Majzlan.

References

Bayliss, P. and Levinson, A. A.: A system of nomenclature for rare-earth mineral species: Revision and extension, Am. Mineral., 73, 422–423, 1988.

Bayliss, P., Kolitsch, U., Nickel, E. H., and Pring, A.: Alunite supergroup: recommended nomenclature, Mineral. Mag., 74, 919–927, 2010.

Biagioni, C., Mauro, D., Pasero, M., Bonaccorsi, E., Lepore, G. O., Zaccarini, F., and Skogby, H.: Crystal-chemistry of sulfates from the Apuan Alps (Tuscany, Italy). VI. Tl-bearing alum-(K) and voltaite from the Fornovolasco mining complex, Am. Mineral., 105, 1088–1098, 2020.

Burton, E. D., Karimian, N., Johnston, S. G., Schoepfer, V. A., Choppala, G., and Lamb, D.: Arsenic-imposed effects on schwertmannite and jarosite formation in Acid Mine Drainage and coupled impacts on arsenic mobility, ACS Earth Space Chem., 5, 1418–1435, 2021.

Bruker AXS Inc.: APEX 3. Bruker Advanced X-ray Solutions, Madison, Wisconsin, USA, 2016.

Cooper, M. A. and Hawthorne, F. C.: Refinement of the crystal structure of zoned philipsbornite-hidalgoite from the Tsumeb mine, Namibia, and hydrogen bonding in the $D^{2+}G_3^{3+}(T^{5+}O_4)(TO_3OH)(OH)_6$ alunite structures, Mineral. Mag., 76, 839–49, 2012.

Dietrich, J. É.: Sur quelques minéraux de la zone d'oxydation du gisement de cuivre de Bou Skour (Anti-Atlas marocain), Thèse, Université de Toulouse, 1970 (in French).

Dietrich, J. É.: La wulfenite de la mine de Bou Skour, quartier de la Patte d'Oie (Jbel Sarhro, Maroc), Notes Serv. géol. Maroc, 32, 25–29, 1972 (in French).

Dietrich, J. É. and Favreau, G.: Bou Skour (Maroc): au pays de wulfénites bleues, Le Cahier des Micromonteurs, 89, 106–114, 2005 (in French).

Dietrich, J. É., Orliac, M., and Permingeat, F.: L'agardite, une nouvelle espèce minérale, et le problème du chlorotile, Bull. Soc. fr. Minéral. Cristallogr., 92, 420–434, 1969 (in French).

Dutrizac, J. E. and Jambor, J. L.: Jarosites and their application in hydrometallurgy, Rev. Mineral. Geochem., 40, 405–452, 2000.

El Azmi, D., Aissa, M., Ouguir, H., Mahdoudi, M.L., El Azmi, M., Ouadjo, A., and Zouhair, M.: Magmatic context of Bou Skour copper deposit (Eastern Anti-Atlas, Morocco): Petrogrography, geochemistry and alterations, J. Afr. Earth Sci., 97, 40–55, 2014.

Ferraris, G. and Ivaldi, G.: Bond valence vs bond length in O···O hydrogen bonds, Acta Crystallogr., B44, 341–344, 1988.

Frost, R. L., Palmer, S. J., Spratt, H. J., and Martens, W. N.: The molecular structure of the mineral beudantite $PbFe_3(AsO_4,SO_4)(OH)_6$ – Implications for arsenic accumulation and removal, J. Molecul. Struct., 988, 52–58, 2011.

Frost, R. L., Xi, Y., Scholz, R., and Tazava, E.: Spectroscopic characterization of the phosphate mineral florencite-La – $LaAl_3(PO_4)_2(OH,H_2O)_6$, a potential tool in the REE mineral prospection, J. Molecul. Struct., 1037, 148–153, 2013.

Gagné, O. C. and Hawthorne, F. C.: Comprehensive derivation of bond-valence parameters for ion pairs involving oxygen, Acta Crystallogr., B71, 562–578, 2015.

Gieré, R., Sidenko, N. V., and Lazareva, E. V.: The role of secondary minerals in controlling the migration of arsenic and metals from high-grade sulfide wastes (Berikul gold mine, Siberia), Appl. Geochem., 18, 1347–1359, 2003.

Grey, I. E., Birch, W. D., Bougerol, C., and Mills, S. J.: Unit-cell intergrowth of pyrochlore and hexagonal tungsten bronze structures in secondary tungsten minerals, J. Solid State Chem., 179, 3834–3843, 2006.

Hatert, F., Lefèvre, P., Pasero, M., and Fransolet, A.-M.: Graulichite-(Ce), a new arsenate mineral from the Stavelot massif, Belgium, Eur. J. Mineral., 15, 733–739, 2003.

Hawthorne, F. C., Krivovichev, S. V., and Burns, P. C.: The crystal chemistry of sulfate minerals. In: Sulfate minerals-crystallography, geochemistry and environmental significance, Rev. Mineral. Geochem., 40, 1–101, 2000.

Holland, T. J. B. and Redfern, S. A. T.: Unit cell refinement from powder diffraction data: The use of regression diagnostics, Mineral. Mag., 61, 65–77, 1997.

Huminicki, D. M. C. and Hawthorne, F. C.: The Crystal Chemistry of Phosphate Minerals, Rev. Mineral. Geochem., 48, 123–253, 2002.

Kampf, A. R., Richards, R. P., Nash, B. P., Murowchick, J. B., and Rakovan, J. F.: Carlsonite, $(NH_4)_5Fe_3^{3+}O(SO_4)_6 \cdot 7H_2O$, and huizingite-(Al), $(NH_4)_9Al_3(SO_4)_8(OH)_2 \cdot 4H_2O$, two new minerals from a natural fire in an oil-bearing shale near Milan, Ohio, Am. Mineral., 101, 2095–2107, 2016.

Kraus, W. and Nolze, G.: Powder Cell – a program for the representation and manipulation of crystal structures and calculation of the resulting X-ray powder patterns, J. Appl. Crystallogr., 29, 301–303, 1996.

Levinson, A. A.: A system of nomenclature for rare-earth minerals, Am. Mineral., 51, 152–158, 1966.

Maacha, L., Ouadjou, A., Azmi, M., Zouhair, M., Saquaque, A., Alansari, A., and Soulaimani, A.: 1.6.-La mine de cuivre et argent de Bouskour (J. Saghro, Anti-Atlas oriental), in: Les principales mines du Maroc, edited by: Mouttaqi, A., Rjimati, E. C., Maacha, L., Michard, A., Soulaimani, A., and Ibouh, H., Nouveaux Guides Géologiques et Miniers du Maroc, 9, 59–64, 2011 (in French).

Majzlan, J., Drahota, P., and Filippi, M.: Parageneses and Crystal Chemistry of Arsenic Minerals, Rev. Mineral. Geochem., 79, 17–184, 2014.

Mandarino, J. A.: The Gladstone-Dale relationship. Part III. Some general applications, Can. Mineral., 17, 71–76, 1979.

Mandarino, J. A.: The Gladstone-Dale relationship. Part IV. The compatibility concept and some application, Can. Mineral., 19, 441–450, 1981.

Martín Romero, F., Prol-Ledesma, R. M., Canet, C., Núñez Alvares, L., and Pérez-Vázquez, R.: Acid drainage at the inactive Santa Lucia mine, western Cuba: Natural attenuation of arsenic, barium

and lead, and geochemical behavior of rare earth elements, Appl. Geochem., 25, 716–727, 2010.

Mauro, D., Biagioni, C., and Zaccarini, F.: A contribution to the mineralogy of Sicily, Italy – Kintoreite from the Tripi mine, Peloritani Mountains: occurrence and crystal structure, Mineral. Mag., https://doi.org/10.1180/mgm.2021.85, online first, 2021.

Mills, S. J., Kartashov, P. M., Kampf, A. R., and Raudsepp, M.: Arsenoflorencite-(La), a new mineral from the Komi Republic, Russian Federation: description and crystal structure, Eur. J. Mineral., 22, 613–621, 2010.

Nickel, E. H. and Temperly, J. E.: Arsenoflorencite-(Ce): a new arsenate mineral from Australia, Mineral. Mag., 51, 605–609, 1987.

Plášil, J., Škoda, R., Fejfavorá, K., Čejka, J., Kasatkin, A., Dušek, M., Talla, D., Lapčák, L., Machovič, V., and Dini, M.: Hydroniumjarosite, $(H_3O)^+Fe_3(SO_4)_2(OH)_6$, from Cerros Pintados, Chile: Single-crystal X-ray diffraction and vibrational spectroscopic study, Mineral. Mag., 78, 535–547, 2014.

Repina, S. A., Popova, V. I., Churin, E. I., Belogub, E. V., and Khiller, V. V.: Florencite-(Sm) – $(Sm,Nd)Al_3(PO_4)_2(OH)_6$: A new mineral species of the alunite-jarosite group from the Subpolar Urals, Geol. Ore Deposti., 53, 564–574, 2011.

Scharm, B., Scharmová, M., Sulovský, B., and Kühn, P.: Philpsbornite, arsenoflorencite-(La), and arsenoflorencite-(Nd) from the uranium district in northern Bohemia, Czechoslovakia, Casopis pro Mineralogii a Geologii, 36, 103–113, 1991.

Shannon, R. D.: Revised effective ionic radii and systematic studies of interatomic distances in halides and chalcogenides, Acta Crystallogr., A32, 751–767, 1976.

Sheldrick, G. M.: Crystal structure refinement with SHELXL, Acta Crystallogr., C71, 3–8, 2015.

Wilson, A. J. C. (Ed.): International Tables for Crystallography Volume C: Mathematical, Physical and Chemical Tables, Kluwer Academic Publishers, Dordrecht, the Netherlands, 1992.